Supporting Information

Different p-Block Elements Induce C_3[111] Octahedral Distortion on Titanium to Generate Intense Nonlinear Effect

Zhenhua Li,‡[a] Zhengli Liang,‡[b] Jiahao Wan,[a] Lehui Liu,[c] Chunxiang Wu,[a] Ping Wang,[a] Xingxing Jiang,*[b] Zheshuai Lin,[b] Hongming Liu*[a]

[a] *Guangxi Key Laboratory of Electrochemical Energy Materials, School of Chemistry and Chemical Engineering, Guangxi University, Nanning, Guangxi 530004, China.*

[b] *Technical Institute of Physics and Chemistry, Chinese Academy of Science, Beijing 100190, China.*

[c] *Key Laboratory of Optoelectronic Materials Chemistry and Physics Fujian Institute of Research on the Fujian 350002, China.*

1. Experimental Section

Experimental Procedures

Reagents. Titanium dioxide (TiO_2, 99.5 %, Sigma Aldrich), tellurium dioxide (TeO_2, 95%, Leyan Reagent), and sulfuric acid (H_2SO_4, 98%, Xiya Reagent) of analytical pure were used without further purification.

Synthesis. Single crystals of $Ti(TeO_3)(SO_4)$ were successfully obtained by hydrothermal reactions. A mixture of TiO_2 (0.799 g, 1.00 mmol), TeO_2 (0.160 g, 1 mmol), H_2SO_4 (1.5 mL), and deionized water (2.0 mL) was put into an autoclave containing poly(tetrafluoroethylene)-lined, heated to 230 ˚C and hold for 48 h, then cooled to ambient temperature at a rate of 3.5 ˚C/h. A possible chemical equation for this reaction should be: $TiO_2+TeO_2+H_2SO_4 \rightarrow Ti(TeO_3)(SO_4)+H_2O$. The reaction product was washed with deionized water and dried at 120 °C, pure colorless transparent needle-shaped crystals of $Ti(TeO_3)(SO_4)$ were isolated in a yield of about 80 % (based on Ti element).

Measurements

Powder X-ray Diffraction (PXRD)

PXRD patterns were collected on a Rigaku D/MAX 2500V diffractometer equipped with Cu k_α radiation (λ=1.540598 Å), in the angular range of 2ϑ from 10° to 70°, with a scan rate of 1 °/min at room temperature.

Energy Dispersive X-ray Spectroscopy (EDS)

Energy-dispersive X-ray spectrometry was performed on a Zeiss Sigma 300 field-emission scanning electron microscope equipped with an X-ray spectroscope (15 kV).

Infrared (IR) spectrum

The powder IR spectrum of the polycrystalline samples was recorded using a Nicolet iS10 Fourier transform IR spectrometer within the wavenumber range of 4000-500 cm^{-1} at room temperature.

Single-Crystal X-ray Diffraction (XRD)

Data collections for the compound were executed on a Bruker SMARTAPEXDUO diffractometer with graphite-monochromated Mo-Kα radiation (λ =0.71073 Å) at 296 (2)K. Data set reduction and integration were accomplished using the SAINTPLUS19 crystallographic software package.[1] The SHELXTL software package[2] was utilized to directly process and refine the structure, and structural refinement was performed using the Olex2 software.[3, 4] After refining several times, reasonable *R* values were gained, and the formula of the compound was determined to be $Ti(TeO_3)(SO_4)$. The space group was checked with PLATON[5] program and no higher symmetry was found. Table S1 summarizes the relevant crystal data and structural refinement information for $Ti(TeO_3)(SO_4)$. Atomic coordinates, isotropic displacement coefficients, selected bond lengths, and bond angles are listed in Table S2-S3. The details of the crystal structure (CCDC 2364994) can be sought from the Cambridge Crystallographic Data Centre at www.ccdc.cam.ac.uk/data_request/cif.

SHG Measurements

Nonlinear optical properties were investigated based on the *Kurtz-Perry* method[6] using a pulsed Q-switched Nd: YAG (λ=1064 nm) laser system. Due to the SHG efficiency being related to particle size, $Ti(TeO_3)(SO_4)$ samples with several particle-size ranges, including 20−40, 40−80, 80−100, 100−125, 125−150, 150−200, and 200−300 μm, were prepared by grinding and sieving synthetic samples. KH_2PO_4 (KDP) microcrystals in the same particle size ranges were served as the references.

Birefringence Measurements

The birefringence of the $Ti(TeO_3)(SO_4)$ sample was measured with a polarizing microscope (MshOt MP41) generating a scale and a white light source. The birefringence was deduced according to Equation (1):[7]

ΔR (retardation) = $\Delta n \times T$ (1)

where ΔR, Δn, T denotes the optical path difference, the birefringence, and the thickness of the crystal, respectively. The positive and negative rotations of compensation render relative retardation. The apparent boundaries between the first-, second-, and third-order interference colors result in a minor deviation. A transparent $Ti(TeO_3)(SO_4)$ crystal sheet was chosen for measurements to improve the accuracy of birefringence.

Thermal analysis

The thermal stability was measured on a Netzsch STA 449F3 thermal analyzer instrument. About 10 mg of powders were placed in an alumina crucible and heated from 25 to 800 °C at a heating rate of 10 °C/min in an N_2 shielding atmosphere.

Water stability analysis

A complete crystal was picked out to soak in deionized water and maintain for 15 days, its morphological change was photographed by a microscope (10×).

UV–Vis–NIR spectrum

The UV-vis-NIR diffuse reflectance spectrum was recorded on a Shimadzu UV-3600i Plus spectrophotometer in 200−800 nm range, with $BaSO_4$ of spectral grade applied as a criterion of 100% reflectance. Reflectance spectrum was transformed into absorption spectrum through the *Kubelka-Munk* function:[8] $F(R)=(1-R)^2/2R$, where R is the reflectance. The band gap is estimated by Tauc method[9] through the following equation: $(F(R)\cdot h\nu)^{1/\gamma}=B(h\nu-E_g)$, where h is the Planck constant, ν is the photon's frequency, E_g is the band gap energy, and B is a constant. The γ factor depends on the nature of the electron transition and is equal to 1/2 or 2 for the direct and indirect transition band gaps, respectively.

Laser-Damage Threshold (LDT) Measurement

The LDTs were measured on the powder samples (150−250 μm) with a pulsed Nd: YAG laser (1064 nm, 10 ns, 1Hz). $AgGaS_2$ samples with the same particle size range were served as the reference. With the energy of the laser emission gradually increased, the sample color changes were observed to determine the damage threshold.

Computational Methods

The electronic structures and optical properties were calculated via a plane-wave pseudopotentials method[10, 11] within density functional theory (DFT) implemented in the total energy code CASTEP.[12] The exchange-correlation energy was treated using the functional CA-PZ developed within the local density approximation (LDA)[13] form. The valence electrons were regarded as O: $2s^2 2p^4$, S: $3s^2 3p^4$, Ti: $3d^2 4s^2$, and Te: $5s^2 5p^4$. An energy cutoff of 850 eV was set and a Monkhorst-Pack[14] *k*-point mesh (6 × 4 × 4) in the first Brillouin zone was used. During the optical property calculations, 210 empty bands were guaranteed to ensure the convergence of linear optical properties and SHG coefficients for $Ti(TeO_3)(SO_4)$. The SHG coefficients d_{ij} were calculated by the formula developed by Lin et al.[15] To deeply understand the contribution of the constituent groups to SHG effect, SHG-weighted electron density analysis was performed based on the crystal structure. For the calculation of refractive index, the band gap (3.97 eV) refered to the UV-cutoff edge of 312 nm was used. Cosidering that the uncoincident between the optical main axis (*X*1, *X*2, *X*3) and the crystallographic main axis (*a*, *b*, *c*) of the monoclinic crystal system, and the *b*-axis of the monoclinic crystal system was one of the optical main axis, the two assumed perpendicular optical axes in the *ac*-plane were repeatedly evaluated and rotated until the change of the birefringence and the phase-matched cutoff wavelength were less than 0.001 and 0.5 nm, respectively. the transformation relationship between the crystal axis (*a*, *b*, *c*) and the optical main axis (*X*1, *X*2, *X*3) was obtained as follows:

$$\begin{pmatrix} X_1 \\ X_2 \\ X_3 \end{pmatrix} = \begin{pmatrix} -0.78 & 0 & 0.62 \\ 0 & 1 & 0 \\ 0.63 & 0 & 0.79 \end{pmatrix} \begin{pmatrix} a \\ b \\ c \end{pmatrix}$$

2. Supporting Figures and Tables

Table S1. Crystallographic Data for $Ti(TeO_3)(SO_4)$.

Formula	$Ti(TeO_3)(SO_4)$
Formula weight	319.56
Temperature(K)	296(2)
Crystal system	Monoclinic
Space group	$P2_1$
a (Å)	4.9516(3)
b (Å)	7.6029(4)
c (Å)	7.1865(4)
α (°)	90
β (°)	105.062(6)
γ (°)	90
Volume ($Å^3$)	261.25(3)
Z	2
Density (calculated)	4.062 g/cm^3
Absorption coefficient	7.487 mm^{-1}
F(000)	292
Reflections collected	2750
Absolute structure parameter	0.01(3)
Independent reflections	1127
Completeness to theta = 25.242°	99.8%
Goodness-of-fit on F^2	0.959
Final *R* indices [I>2σ(I)]	R_1 = 0.0230, wR_2 = 0.0495
R indices (all data)	R_1 = 0.0242, wR_2 = 0.0506

$R_1 = \sum||F_o|-|F_c||/\sum|F_o|$; $wR_2 = [\sum w(Fo^2-Fc^2)^2]/\sum w(Fo^2)^2]^{1/2}$

Table S2. Atomic coordinates (× 10^4) and equivalent isotropic displacement parameters ($Å^2$ × 10^3) for $Ti(TeO_3)(SO_4)$. Ueq is defined as one-third of the trace of the orthogonalized U_{ij} tensor.

atom	Wyck.	x	y	z	U(eq)	BVS
Te(1)	2a	781(1)	5805(1)	4099(1)	10(1)	3.96
Ti(1)	2a	7491(3)	6435(2)	7532(2)	8(1)	4.34
S(1)	2a	6226(4)	2585(3)	9435(3)	10(1)	6.07
O(1)	2a	3942(10)	2751(8)	10396(9)	14(1)	2.23
O(2)	2a	8555(11)	1529(8)	10583(8)	14(1)	2.10
O(3)	2a	5191(10)	1759(8)	7551(8)	19(1)	2.38
O(4)	2a	7293(12)	4372(8)	9258(9)	18(1)	2.08
O(5)	2a	3880(10)	6259(7)	6139(8)	13(2)	1.56
O(6)	2a	8792(10)	4972(8)	5849(7)	14(1)	2.02
O(7)	2a	8311(12)	8493(7)	6411(9)	18(1)	2.51

Table S3. Selected bond lengths (Å) for $Ti(TeO_3)(SO_4)$.

Lengths (Å)			
Te(1)−O(5)	1.858(5)	Ti(1)−O(6)	1.876(5)
Te(1)−O(6)$^{\#1}$	1.897(5)	Ti(1)−O(7)	1.852(6)
Te(1)−O(7)$^{\#2}$	1.874(6)	S(1)−O(1)	1.476(5)
Ti(1)−O(1)$^{\#3}$	2.066(6)	S(1)−O(2)	1.470(6)
Ti(1)−O(2)$^{\#4}$	2.072(6)	S(1)−O(3)	1.459(6)
Ti(1)−O(4)	2.018(6)	S(1)−O(4)	1.475(6)
Ti(1)−O(5)	1.813(5)		

Symmetry transformations used to generate equivalent atoms: #1 x-1,y,z ; #2 -x+1,y-1/2,-z+1; #3 -x+1,y+1/2,-z+2; #4 -x+2,y+1/2,-z+2

Table S4. Calculated SHG coefficients of $Ti(TeO_3)(SO_4)$.

SHG tensor components	Values (pm/V)	SHG tensor components	Values (pm/V)
d_{111}	0	d_{133}	0
d_{112}	0.66	d_{222}	3.16
d_{113}	0	d_{223}	0
d_{122}	0	d_{233}	-0.99
d_{123}	-1.84	d_{333}	0

Table S5. Calculated dipole moment component of $Ti(TeO_3)(SO_4)$.

unit	Diplole moment (D=Debyes)			
	x	y	z	total magnitude
TiO_6	0.173	-1.112	3.629	3.800
$Ti^{\#1}O_6$	-0.173	-1.112	-3.629	3.800
TiO_6 in cell	0.000	-2.224	0.000	
TeO_3	2.239	-7.921	9.067	12.245
$Te^{\#1}O_3$	-2.239	-7.921	-9.067	12.245
TeO_3 in cell	0	-15.842	0	
SO_4	-0.482	0.597	-0.217	0.798
$S^{\#1}O_4$	0.482	0.600	0.217	0.798
SO_4 in cell	0	1.197	0	
Net dipole moment	0	-16.867	0	16.867

Symmetry transformations used to generate equivalent atoms: #1 1-x, $\pm$ 0.5+y, 1-z;

Table S6. Calculated dipole moment component of $KTiOPO_4$.

unit	Symmetry transformations	Diplole moment (D=Debyes)			
		x	y	z	total magnitude
$Ti(1)O_6$	0.5+x, 0.5-y, z	2.515	1.639	3.301	4.462
$Ti(1)O_6$	x, y, z	2.518	-1.639	3.302	4.464
$Ti(1)O_6$	1-x, 1-y, 0.5+z	-2.515	1.637	3.302	4.461
$Ti(1)O_6$	0.5-x, 0.5+y, 0.5+z	-2.515	-1.640	3.300	4.462
$Ti(2)O_6$	x, y, z	1.543	1.582	2.328	3.209
$Ti(2)O_6$	0.5-x, -0.5+y, 0.5+z	-1.543	1.584	2.329	3.211
$Ti(2)O_6$	1-x, 1-y, 0.5+z	-1.543	-1.582	2.328	3.210
$Ti(2)O_6$	0.5+x, 1.5-y, z	1.542	-1.584	2.328	3.211
TiO_6 in cell		0	0	22.517	
$P(1)O_4$	1.5-x, -0.5+y, 0.5+z	0.433	-0.096	1.277	1.352
$P(1)O_4$	0.5+x, 1.5-y, z	-0.431	0.097	1.281	1.355
$P(1)O_4$	1-x, 1-y, 0.5+z	0.430	0.097	1.277	1.351
$P(1)O_4$	x, y, z	-0.429	-0.098	1.280	1.353
$P(2)O_4$	1-x, 1-y, -0.5+z	-0.403	-0.228	0.245	0.524
$P(2)O_4$	0.5-x, -0.5+y,-0.5+z	-0.403	0.230	0.243	0.524
$P(2)O_4$	x, y, z	0.404	0.225	0.246	0.524
$P(2)O_4$	0.5+x, 1.5-y, z	0.402	-0.232	0.246	0.525
PO_4 in cell		0	0	6.094	
Net dipole moment		0	0	28.611	28.611

Table S7. Space groups, SHG responses and birefringence information of some sulfates.

Number	Compounds	Space Group	SHG intensity (× KDP)	Birefringence	Reference
1	$(NH_4)_2BeS_2O_8$	$I\bar{4}2d$	1.01	0.0175@546 nm	[16]
2	$La(NH_4)(SO_4)_2$	$Pmn2_1$	2.4	0.03@1064 nm	[17]
3	$[Ag(NH_3)_2]_2SO_4$	$P\bar{4}2_1c$	1.4	0.080@589 nm	[18]
4	$CsSbF_2SO_4$	$Pna2_1$	3	0.112@1064 nm	[19]
5	$(NH_4)_2Bi_2(SO_4)_2Cl_4$	$P2_12_12_1$	4.8	0.055@1064 nm	[20]
6	$K_2Bi_2(SO_4)_2Cl_4$	$P2_12_12_1$	5.5	0.056@1064 nm	[20]
7	$Rb_2Bi_2(SO_4)_2Cl_4$	$P2_12_12_1$	5.3	0.047@1064 nm	[20]
8	$K_4Sb(SO_4)_3Cl$	$P6_1$	0.1	0.068@546 nm	[21]
9	$KBiCl_2SO_4$	$P2_12_12_1$	1.7	0.098@1064 nm	[22]
10	$CeF_2(SO_4)$	$Pca2_1$	8	0.361@546 nm	[23]
11	$ZrF_2(SO_4)$	$Pca2_1$	3.2	0.044@546 nm	[24]
12	$HfF_2(SO_4)$	$Pca2_1$	2.5	0.045@546 nm	[24]
13	$Ce_3F_4(SO_4)_4$	$C2$	1	0.141@546 nm	[25]
14	$In_3(SO_4)(TeO_3)_2F_3(H_2O)$	$P2_12_12_1$	0.11	0.088@1064 nm	[26]
15	$NaCe(SO_4)_2(H_2O)$	$P3_12_1$	0.2	0.039@546 nm	[27]
16	$NaBi(SO_4)_2(H_2O)$	$P3_22_1$	0.38	0.062@546 nm	[27]
17	$Rb_3In(SO_4)_3$	$R3c$	0.5	0.019@1064 nm	[28]
18	$Te(CS(NH_2)_2)_4SO_4{\cdot}2H_2O$	Cc	2.4	0.210@546 nm	[29]
19	$Te_2O_3(SO_4)$	$Pmn2_1$	6	0.043@546 nm	[30]
20	$Te(OH)_3(SO_4){\cdot}H_3O$	$P2_12_12_1$	3	0.052@546 nm	[30]
21	$NH_4NaLi_2(SO_4)_2$	$P6_3$	1.1	0.009@546 nm	[31]
22	$LiKSO_4$	$P6_3$	4	0.0002@546 nm	[32]
23	$Ce(IO_3)_2SO_4$	$P2_12_12_1$	3.5	0.259@546 nm	[33]
24	$Hg_2(IO_3)_2(SO_4){\cdot}H_2O$	$C2$	6	0.125@1064 nm	[34]
25	$Nb_2O_3(IO_3)_2(SO_4)$	$P2_1$	6	0.220@1064 nm	[35]
26	$Sb_6O_7(SO_4)_2$	$Ccc2$	2	0.052@1064nm	[36]
27	$Hg_3O_2SO_4$	$P3_221$	14	0.100@546 nm	[37]
28	$NaHSO_4{\cdot}H_2O$	Cc	1.5	0.042@546 nm	[38]
29	$HgSO_4$	$Pmn2_1$	11	0.093@546 nm	[39]
30	$Ti(TeO_3)(SO_4)$	$P2_1$	11.6	0.145@visible light	**This work**

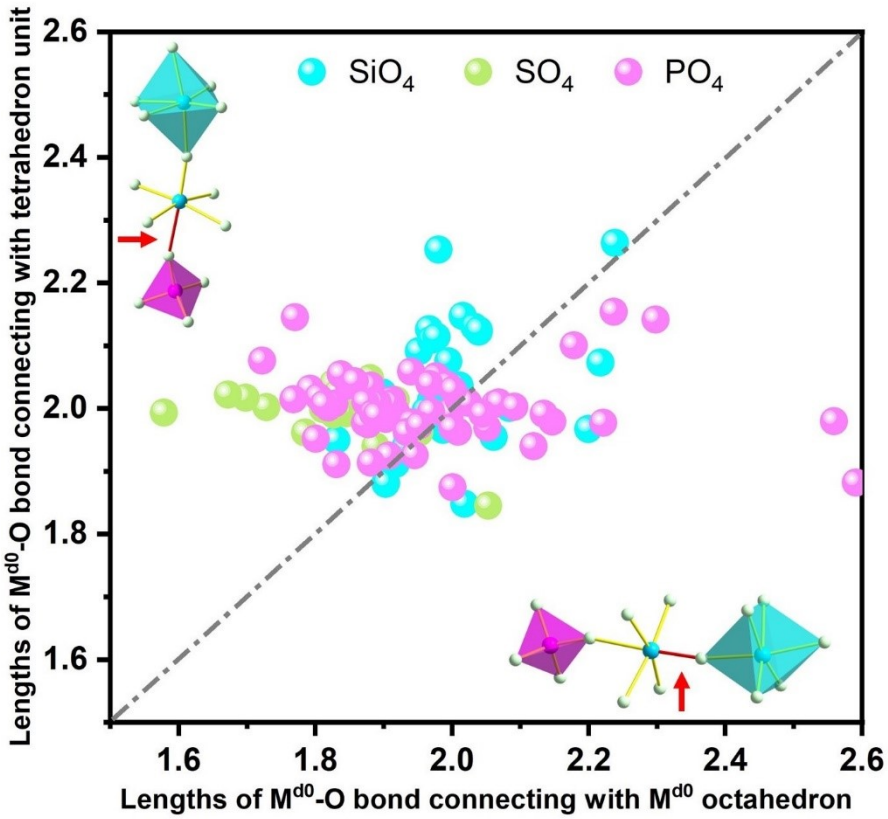

Figure S1. Length distribution of M^{d0}–O bonds in the [$M^{d0}O_6$] octahedron connected to other [$M^{d0}O_6$] octahedra and tetrahedral units simultaneously in phosphates, sulfates, and silicates containing M^{d0}. The data are from the structures in the Inorganic Crystal Structure Database (ICSD), and those compounds with disorder or of doped are not included. The *x*-axis represents the average lengths of the M^{d0}–O bonds connected to [$M^{d0}O_6$] octahedra, and the *y*-axis represents the average lengths of the M^{d0}–O bonds connected to tetrahedral units in the same [$M^{d0}O_6$] octahedron (the different tetrahedral units have been presented by different colour codes). The coordinate points located on the diagonal means that for these [$M^{d0}O_6$] octahedra, the average length of the M^{d0}–O bonds connected with [$M^{d0}O_6$] octahedra is equal to that connected with the tetrahedral units. It seems that the majority of the coordinate points deviate from the diagonal, implying that inside the [$M^{d0}O_6$] octahedra, the length of the M^{d0}–O bonds connecting to the tetrahedral groups differes greatly from that connecting to [$M^{d0}O_6$] octahedron, which induces universal distortion inside the [$M^{d0}O_6$] octahedra.

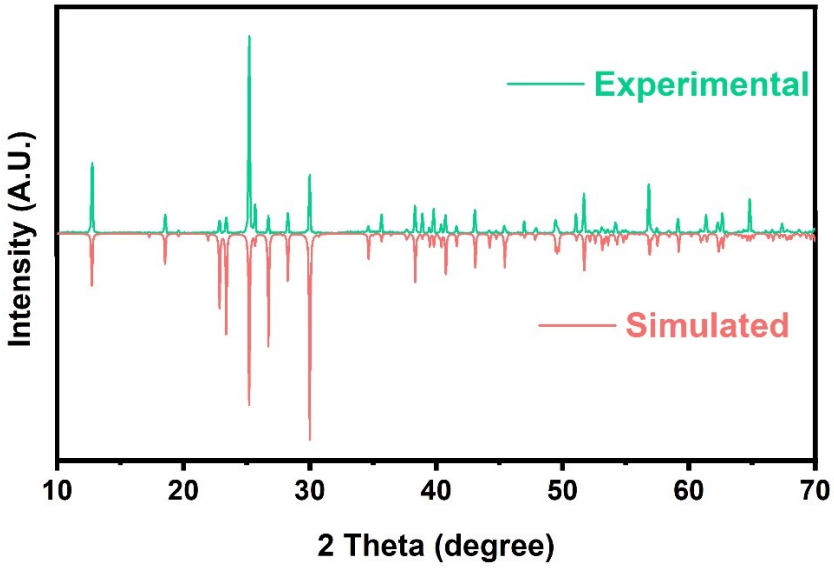

Figure S2. Simulated and experimental powder X-ray diffraction patterns of $Ti(TeO_3)(SO_4)$.

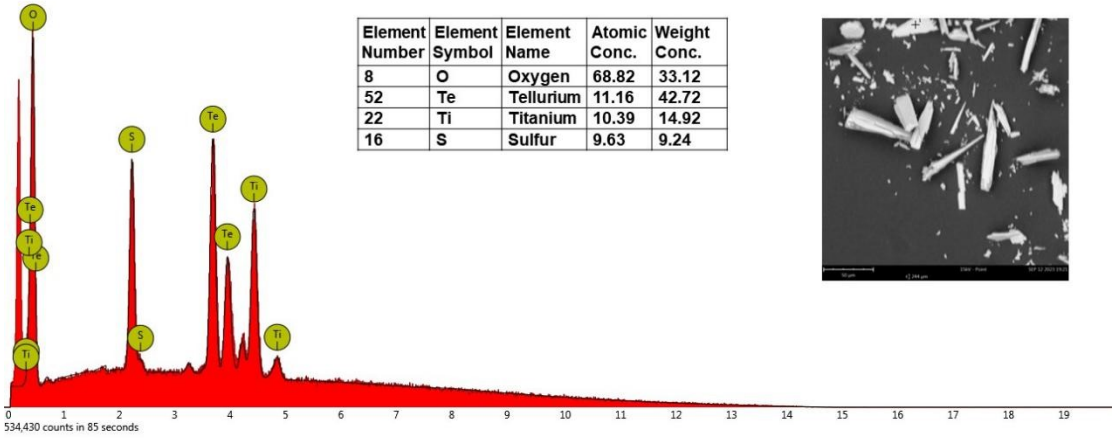

Element Number	Element Symbol	Element Name	Atomic Conc.	Weight Conc.
8	O	Oxygen	68.82	33.12
52	Te	Tellurium	11.16	42.72
22	Ti	Titanium	10.39	14.92
16	S	Sulfur	9.63	9.24

Figure S3. The EDS analysis result of $Ti(TeO_3)(SO_4)$.

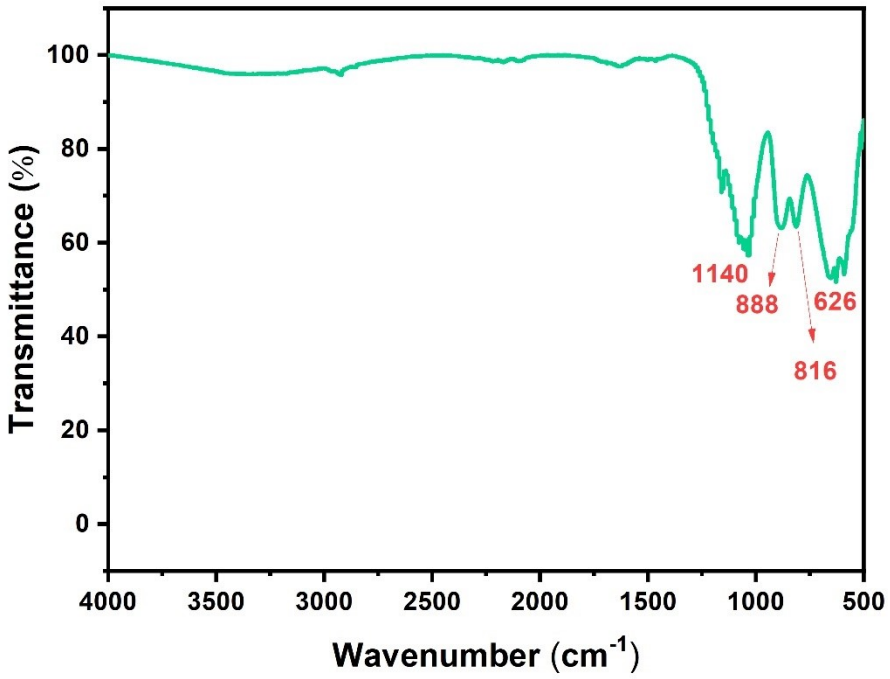

Figure S4. Infrared spectrum of $Ti(TeO_3)(SO_4)$.

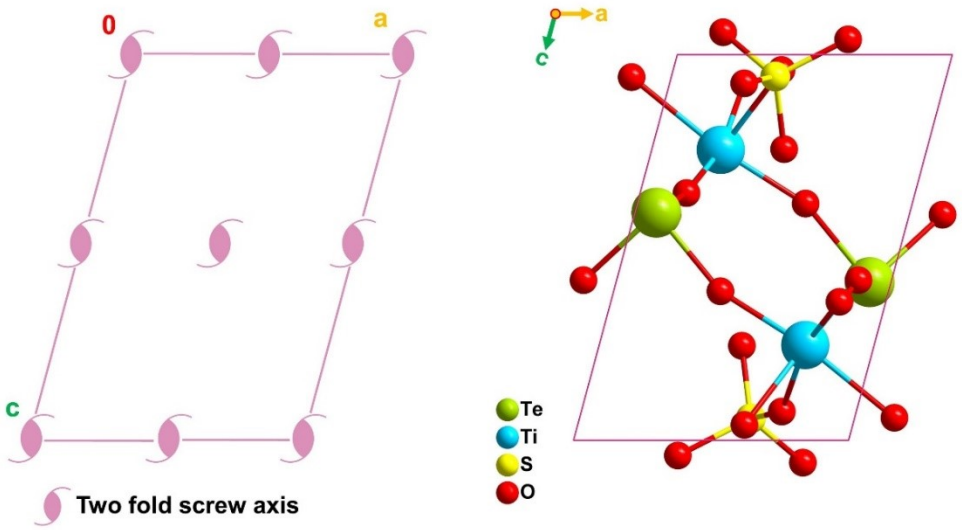

Figure S5. Symmetrical elements diagram (left) and unit cell content (right) for $Ti(TeO_3)(SO_4)$.

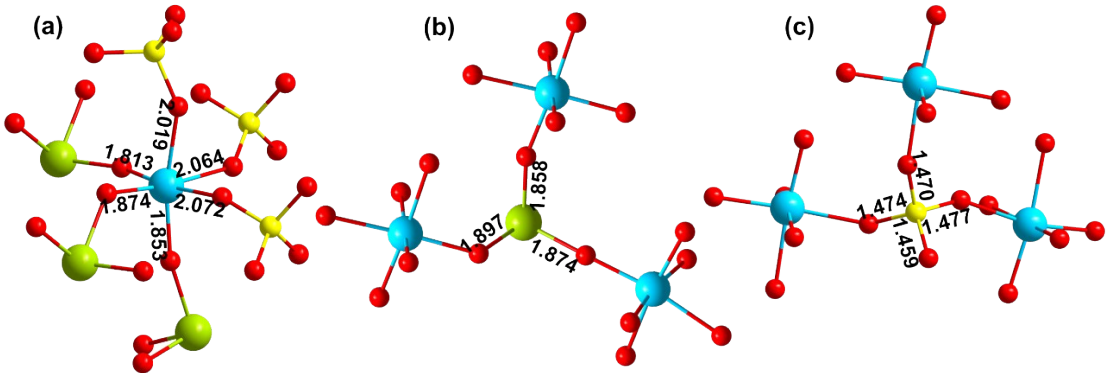

Figure S6. The coordination environment of anionic groups: [TiO_6] (a), [TeO_3] (b), and [SO_4] (c).

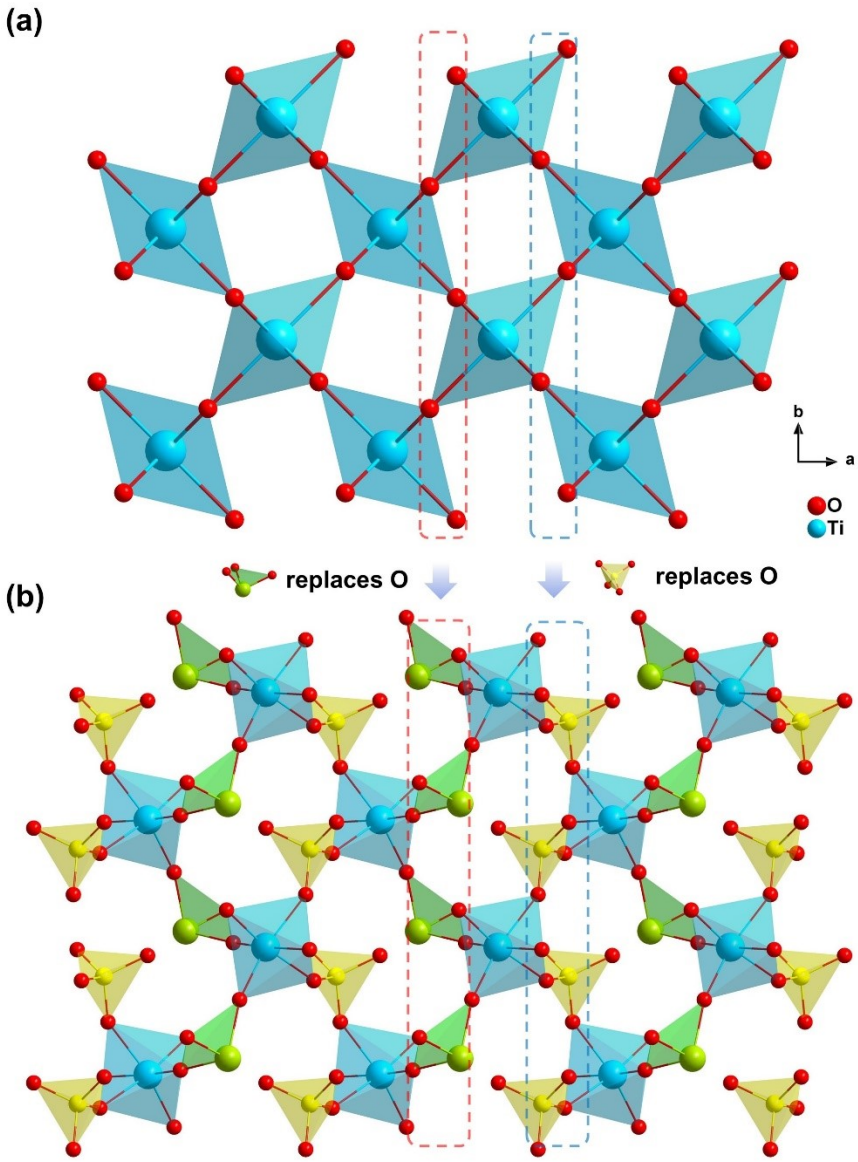

Figure S7. The structural evolution from TiO_2 ($P4_2/mnm$ space group, no. 136) to $Ti(TeO_3)(SO_4)$: (a) the structure of TiO_2 viewing along the *c*-axis, (b) the structure of $Ti(TeO_3)(SO_4)$.

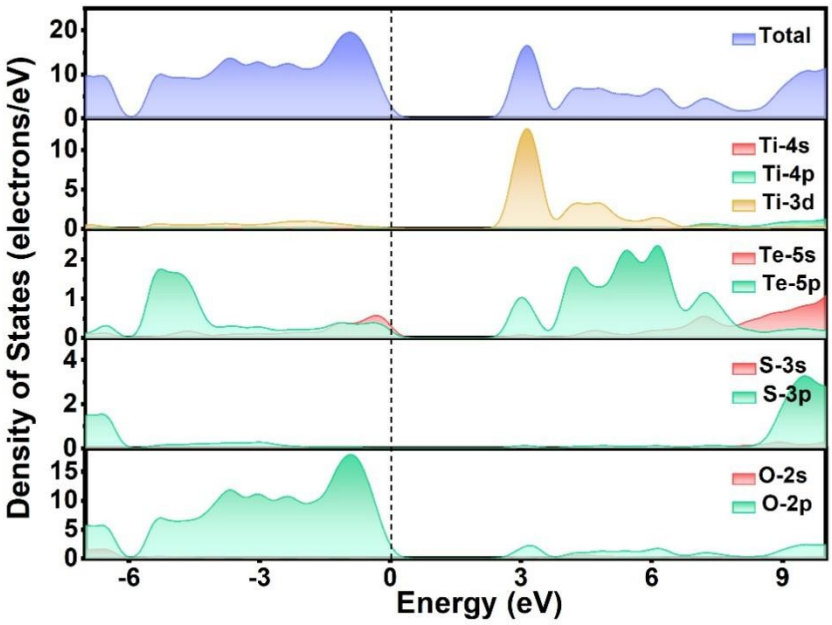

Figure S8. Calculated partial and total density of states of $Ti(TeO_3)(SO_4)$.

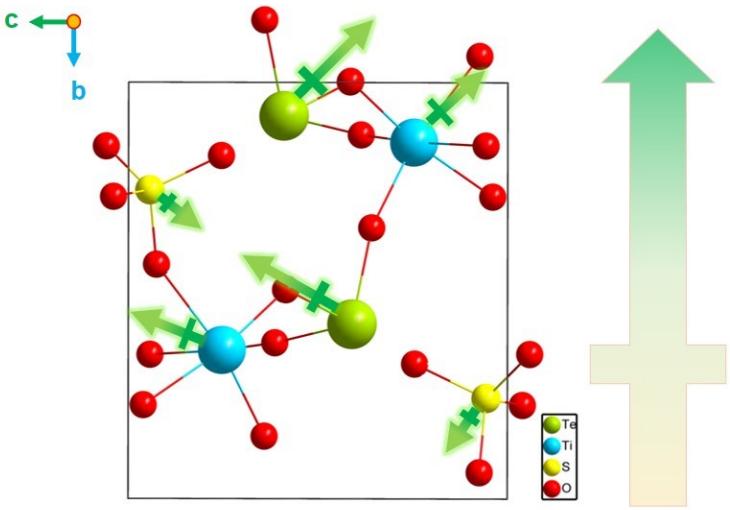

Figure S9. Calculated dipole moment magnitude and direction of the [TeO_3], [TiO_6], and [SO_4] units in Ti(TeO_3)(SO_4).

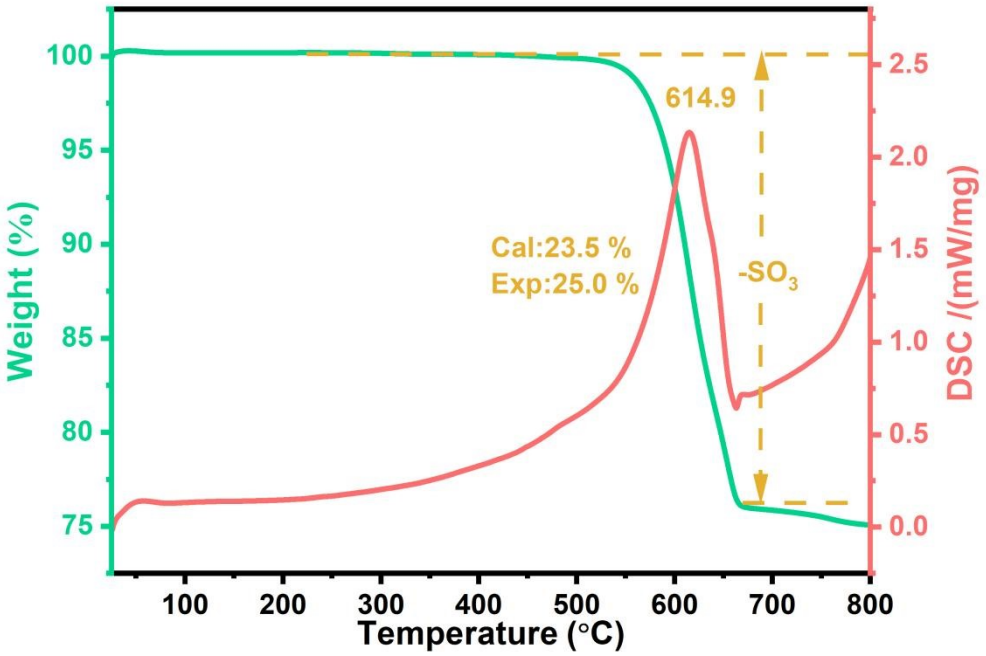

Figure S10. The TGA and DSC curves for $Ti(TeO_3)(SO_4)$.

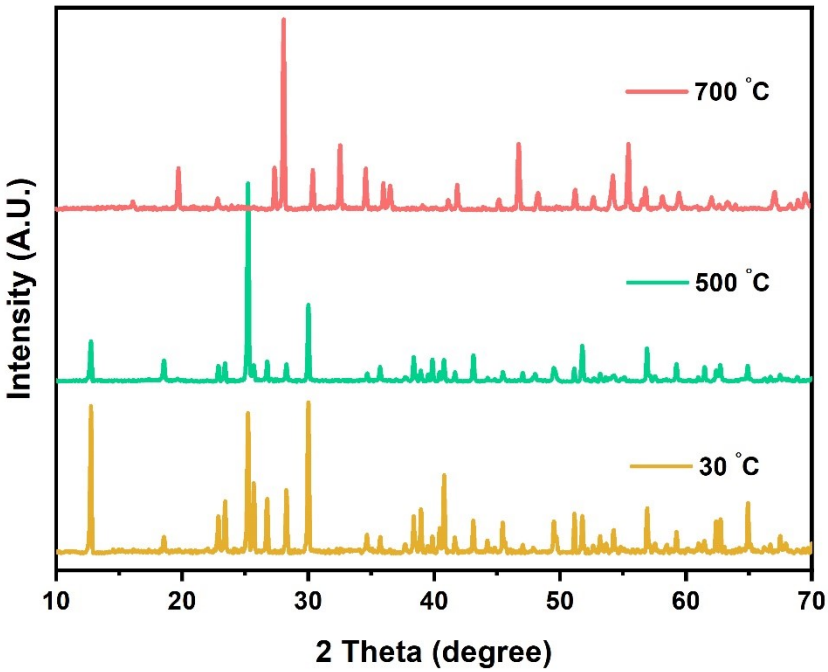

Figure S11. Powder X-ray diffraction patterns of residues in different temperature for $Ti(TeO_3)(SO_4)$.

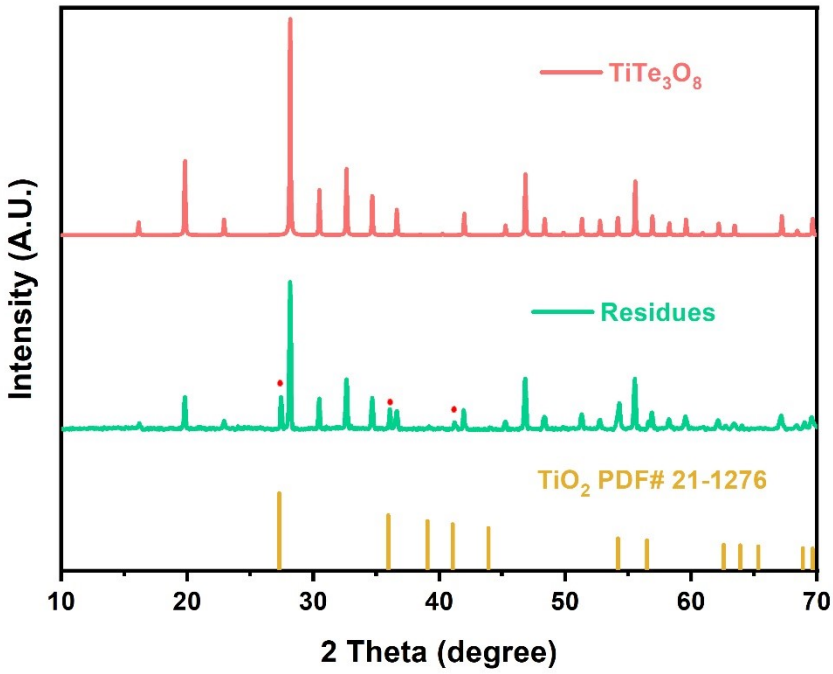

Figure S12. Powder X-ray diffraction patterns of the thermal decomposition residues of $Ti(TeO_3)(SO_4)$ at 700 °C.

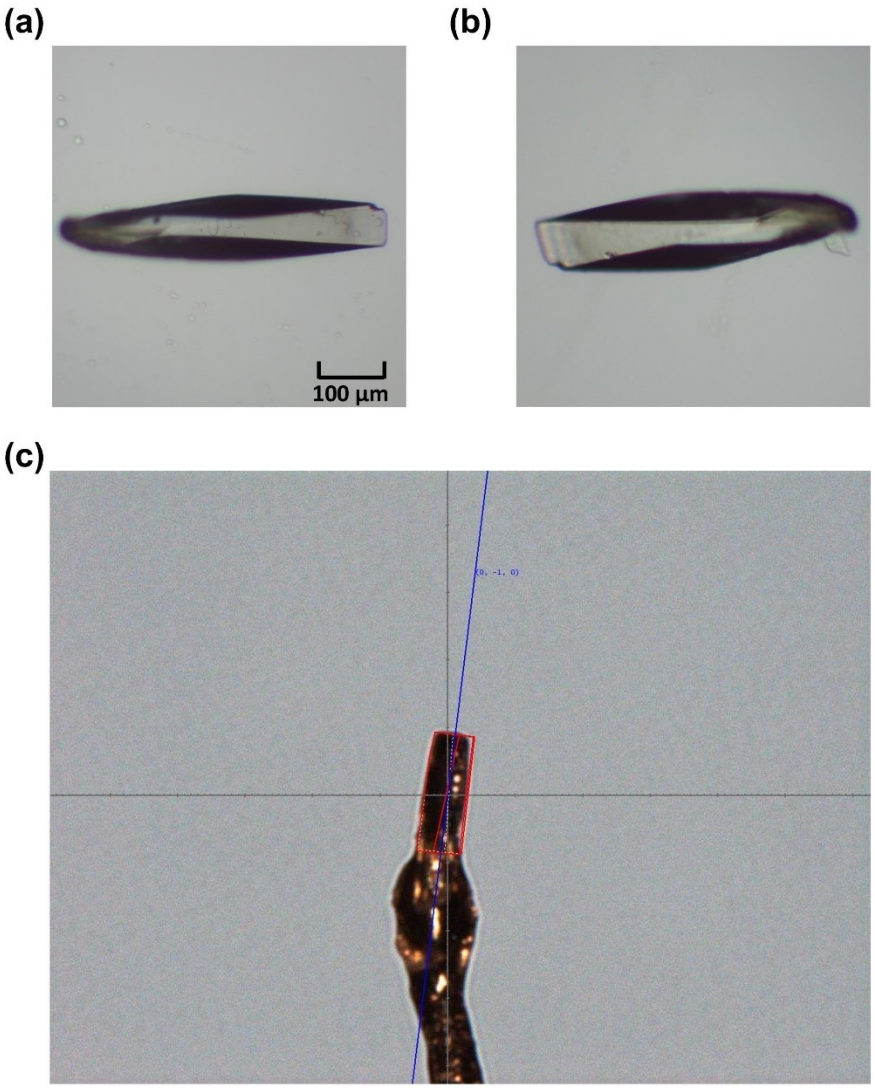

Figure S13. The fresh $Ti(TeO_3)(SO_4)$ crystal (a) and the crystal soaked in water for 15 days (b); (c) Crystal orientation determined by the single-crystal XRD on an Synergy Custom system diffractometer (the spontaneously grown crystal realizes the longest extension along the *b*-axis).

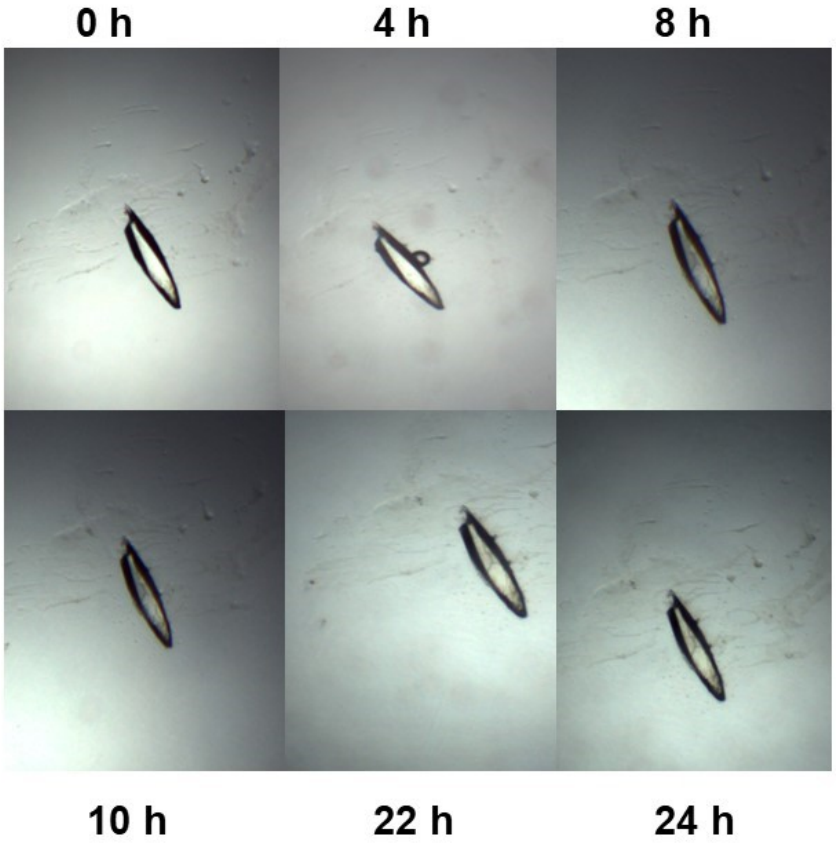

Figure S14. Evolution of the $Ti(TeO_3)(SO_4)$ crystal soaked in 0.1 mol/L HNO_3 for 24 h.

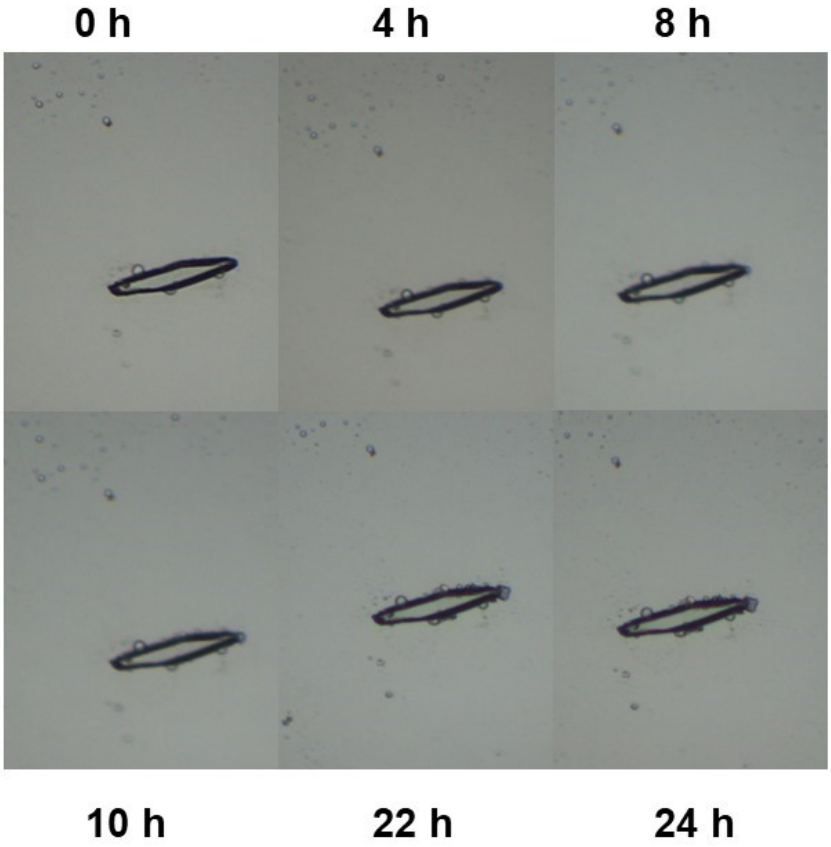

Figure S15. Evolution of the $Ti(TeO_3)(SO_4)$ crystal soaked in 0.1 mol/L NaOH for 24 h.

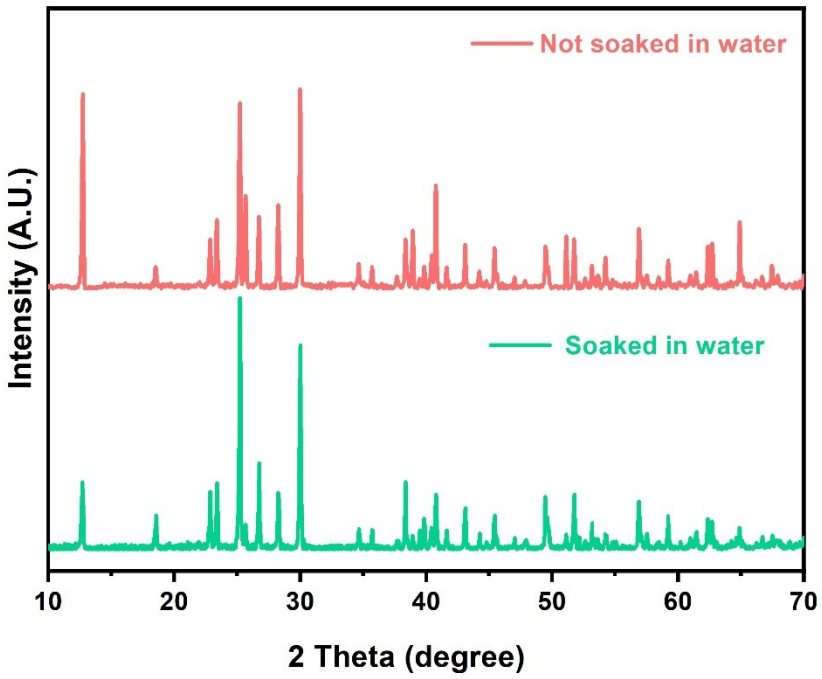

Figure S16. The powder XRD patterns of $Ti(TeO_3)(SO_4)$ of fresh samples and samples after soaked in water for 15 days.

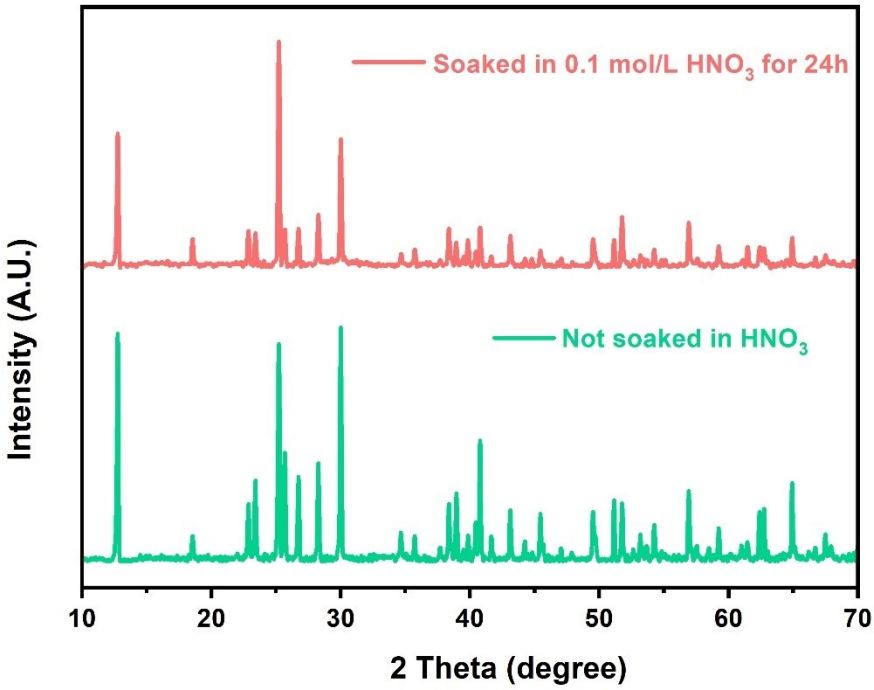

Figure S17. The powder XRD patterns of $Ti(TeO_3)(SO_4)$ of fresh samples and samples after soaked in 0.1 mol/L HNO_3 for 24 h.

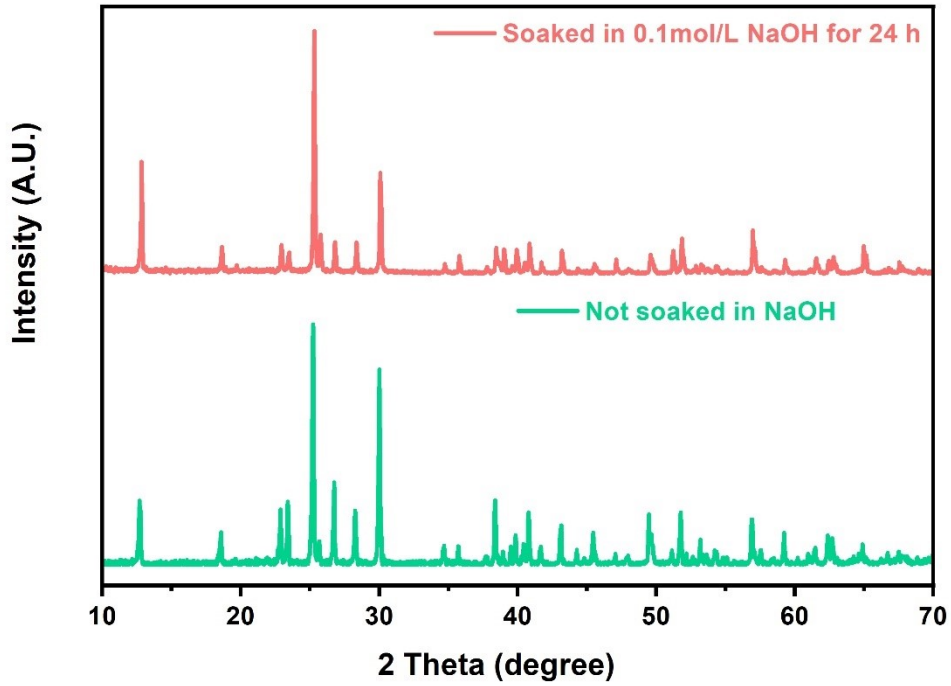

Figure S18. The powder XRD patterns of $Ti(TeO_3)(SO_4)$ of fresh samples and samples after soaked in 0.1 mol/L NaOH for 24 h.

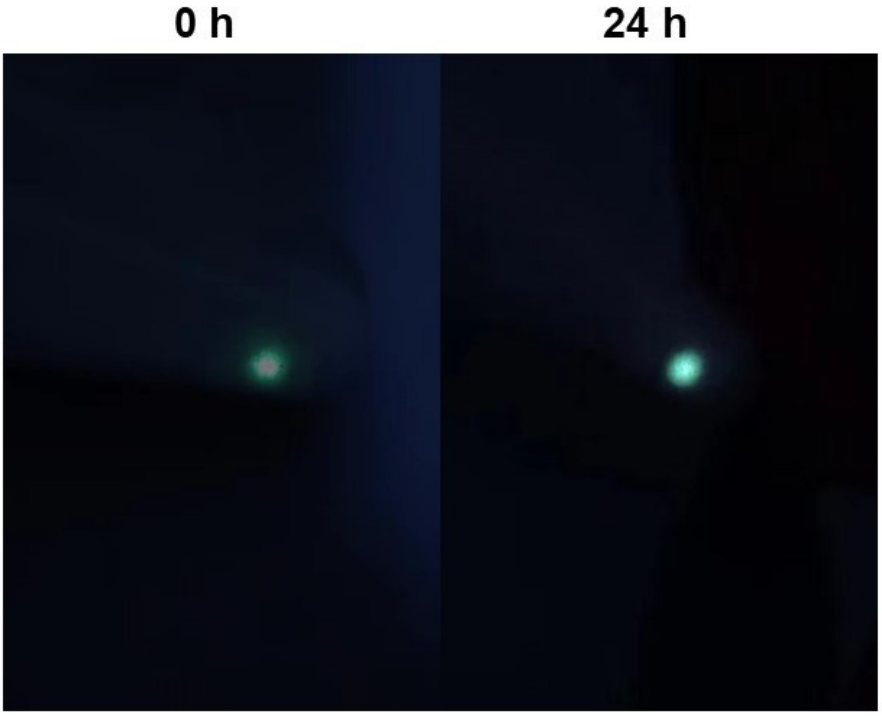

Figure S19. Observed 532 nm laser output based on the fresh $Ti(TeO_3)(SO_4)$ crystal and samples soaked in 0.1 mol/L HNO_3 for 24 h.

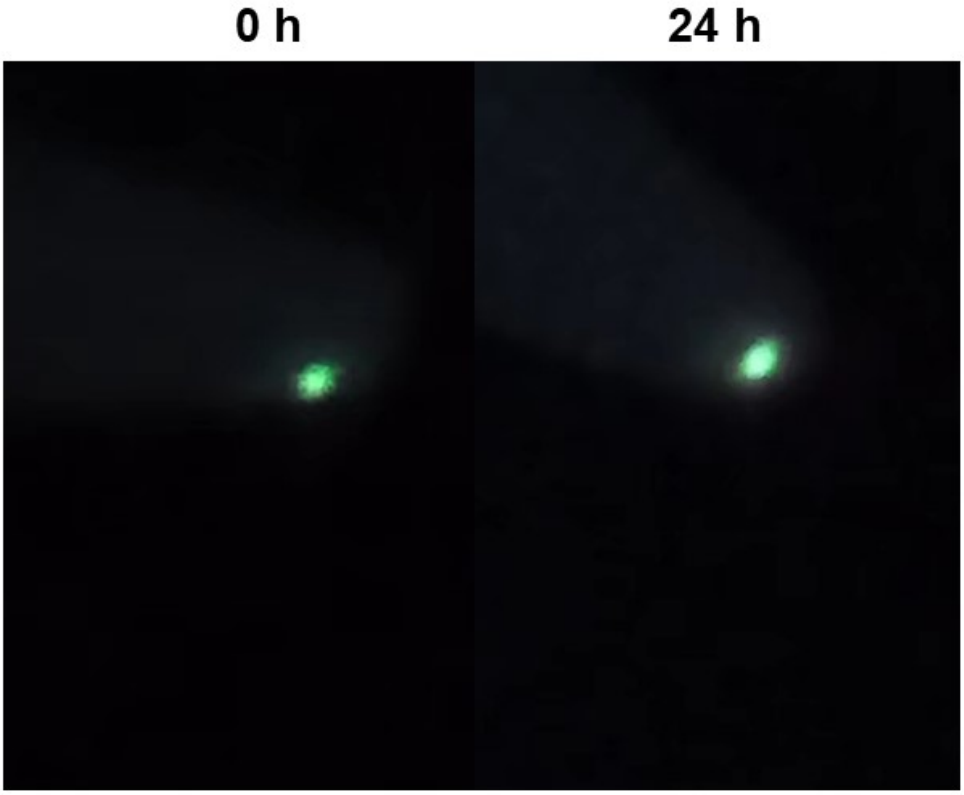

Figure S20. Observed 532 nm laser output based on the fresh $Ti(TeO_3)(SO_4)$ crystal and samples soaked in 0.1mol/L NaOH for 24 h.

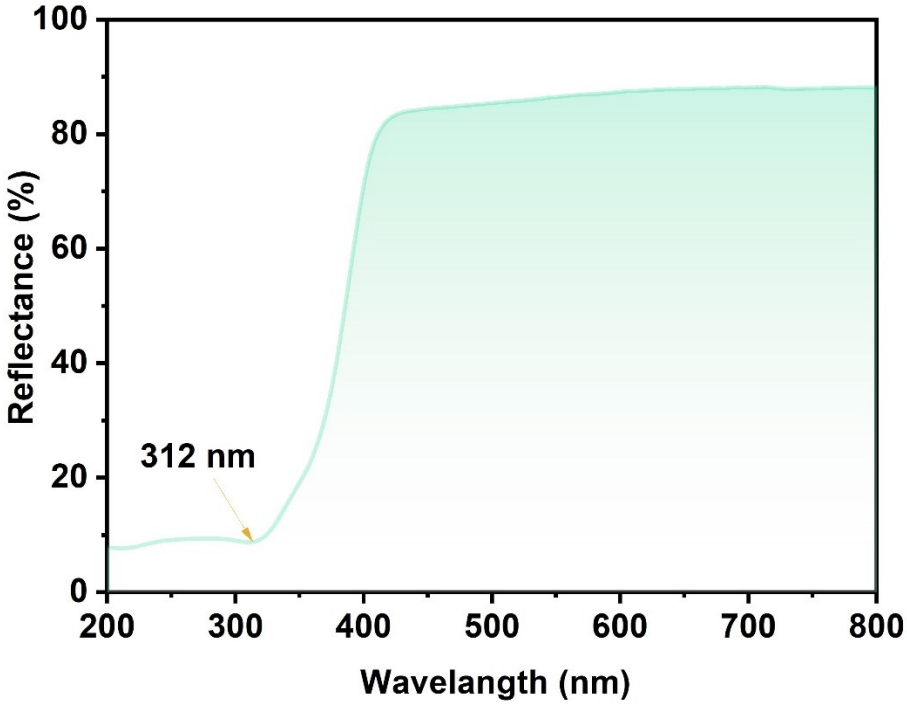

Figure S21. UV-Vis-NIR diffuse reflectance spectrum of $Ti(TeO_3)(SO_4)$.

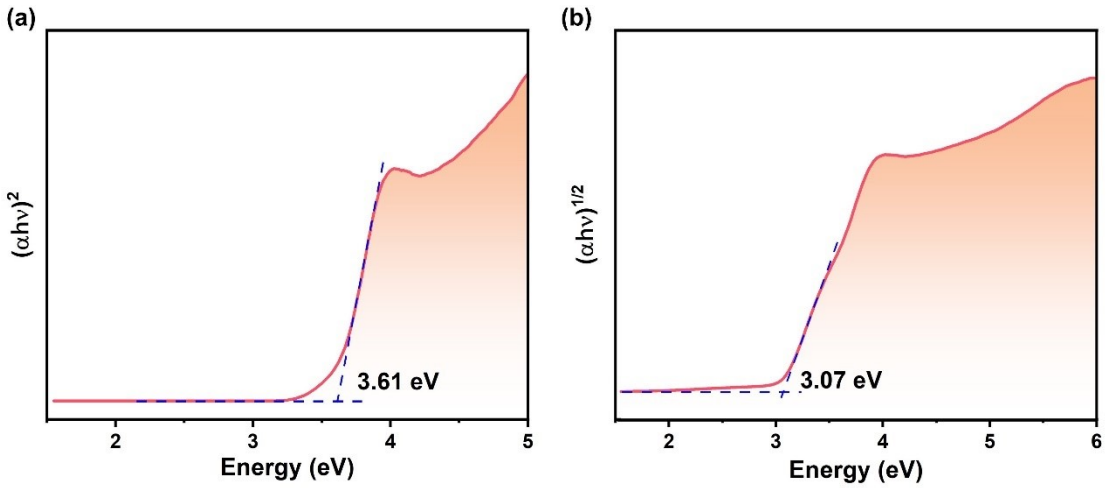

Figure S22. The band gap of $Ti(TeO_3)(SO_4)$ determined by Tauc plot based on UV-Vis-NIR diffuse reflectance spectrum: (a) direct band gap, (b) indirect band gap.

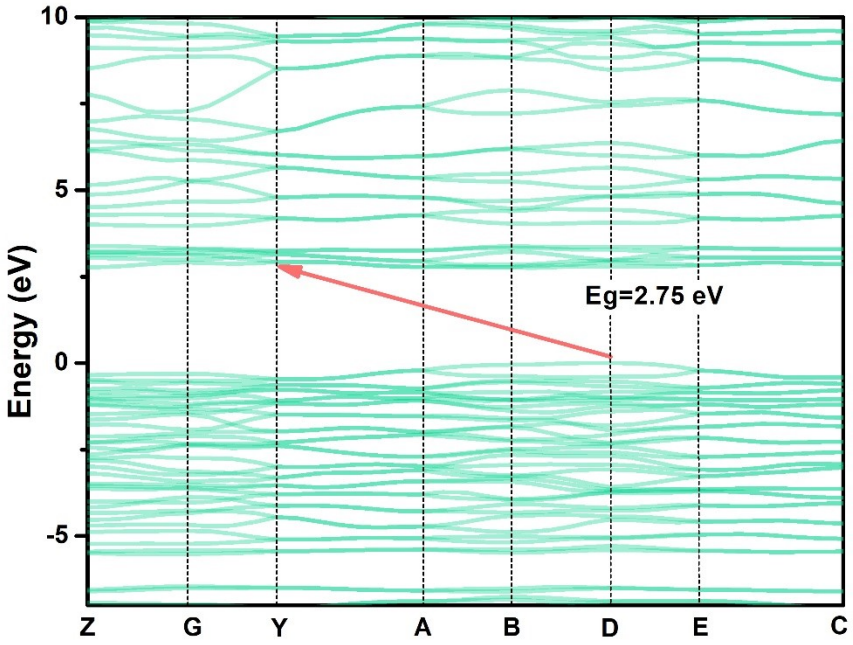

Figure S23. Calculated electronic band structure of $Ti(TeO_3)(SO_4)$.

3. References:

[1] V. SAINT, Inc., Madison, WI, 2008.

[2] G. Sheldrick, *Acta Crystallogr. A,* 2008, **64**, 112−122.

[3] O. V. Dolomanov, L. J. Bourhis, R. J. Gildea, J. A. K. Howard, H. Puschmann, *J. Appl. Crystallogr.,* 2009, **42**, 339−341.

[4] G. M. Sheldrick, *Acta Crystallogr. C,* 2015, **A71**, 3−8.

[5] Spek, A. *J. Appl. Crystallogr.,* 2003, **36**, 7−13.

[6] S. K. Kurtz, Perry. T. T, *J. Appl. Phys.,* 1968, **39**, 3798−3813.

[7] P. A. Wilks, *Science,* 1966, **154**, 143.

[8] B. E. Sørensen, *Eur. J. Mineral.,* 2012, **25**, 5−10.

[9] W. Macyk, *J. Phys. Chem. Lett.* 2018, **9**, 6814−6817.

[10] E.J. Baerends, *Theor. Chem. Acc.,* 2000, **103**, 265−269.

[11] M. C. Payne, M. P. Teter, D. C. Ailan, *Rev. Mod. Phys.,* 1992, **64**, 1045−1097.

[12] S. J. Clark, M. D. Segall, C. J. Pickard, P. J. Hasnip, M. I. J. Probert, K. Refson, M. C. Payne, *Z. Krist.-Cryst. Mater.,* 2005, **220**, 567−570.

[13] R. Asahi, W. Mannstadt, A. J. Freeman, *Phys. B: Condensed Matter,* 1999, **59**, 7486−7492.

[14] H. J. Monkhorst, J. D. Pack, *Phys. Rev. B,* 1976, **13**, 5188−5192.

[15] R. He, Z. S. Lin, M. H. Lee, C. T. Chen, *J. Appl. Phys.,* 2011, **109**, 103510.

[16] Y. S. Sun, C. S. Lin, H. T. Tian, Y. Q. Zhou, J. D. Chen, S. D. Yang, N. Ye, M. Luo, *Chem. Mater.,* 2022, **34**, 3781−3788.

[17] C. Wu, X. X. Jiang, Y. L. Hu, C. B. Jiang, T. H. Wu, Z. S. Lin, Z. P. Huang, M. G. Humphrey, C. Zhang, *Angew. Chem. Int. Ed.,* 2022, **61**, e202115855.

[18] Y. C. Yang, X. Liu, J. Lu, L. M. Wu, L. Chen, *Angew. Chem. Int. Ed.,* 2021, **60**, 21216−21220.

[19] X. H. Dong, L. Huang, C. F. Hu, H. M. Zeng, Z. E. Lin, X. Wang. K. M. Ok, G. H. Zou, *Angew. Chem. Int. Ed.,* 2019, **58**, 6528−6534.

[20] K. C. Chen, Y. Yang, G. Peng, S. D. Yang, T. Yan, H. X. Fan, Z. S. Lin, N. Y, *J. Mater. Chem. C,* 2019, **7**, 9900−9907.

[21] F. Yang, L. Wang, Y. W. Ge, L. Huang, D. J. Gao, J. Bi, G. H. Zou, *J. Alloys Compd.,* 2020, **834**, 155154.

[22] Z. H. Yue, Z. T. Lu, H. G. Xue, S. P. Guo, *Cryst. Growth Des.,* 2019, **19**, 3843−3850.

[23] C. Wu, T. H. Wu, X. X. Jiang, Z. J. Wang, H. Y. Sha, L. L, Z. S. Lin, Z. P. Huang, X. F. Long, M. G. Humphrey, C. Zhang, *J. Am. Chem. Soc.,* 2021, **143**, 4138−4142.

[24] C. Wu, C. B. Jiang, G. F. Wei, X. X. Jiang, Z. J. Wang, Z. S. Lin, Z. P. Huang, M. G. Humphrey, C. Zhang, *J. Am. Chem. Soc.,* 2023, **145**, 3040−3046.

[25] T. H. Wu, X. X. Jiang, C. Wu, Z. S. Lin, Z. P. Huang, M. G. Humphrey, C. Zhang, *Inorg. Chem. Front.,* 2023, **10**, 5270−5277.

[26] Y. P Gong, Y. X. Ma, S. M. Ying, J. G. Mao, F. Kong, *Inorg. Chem.,* 2019, **58**, 11155−11163.

[27] Y. W. Lu, X. X. Jiang, C. Wu, L. Lin, Z. P. Huang, Z. S. Lin, M. G. Humphrey, C. Zhang, *Inorg. Chem.,* 2021, **60**, 5851−5859.

[28] Q. K. Xu, X. X. Jiang, C. Wu, L. Lin, Z. P. Huang, Z. S. Lin, M. G. Humphrey, C. Zhang, *J. Mater. Chem. C,* 2021, **9**, 5124−5131.

[29] X. Y. Weng, C. S. Lin, G. Peng, H. X. Fan, X. Zhao, K. C. Chen, M. Luo, N. Ye, *Cryst. Growth Des.,* 2021, **21**, 2596−2601.

[30] Y. X. Song, X. Hao, C. S. Lin, D. H. Lin, M. Luo, N. Ye, *Inorg. Chem.,* 2021, **60**, 11412−11418.

[31] Y. Q. Li, F. Liang, S. G. Zhao, L. N. Li, Z. Y. Wu, Q. R. Ding, S. Liu, Z. S. Lin, M. C. Hong, J. H. Luo, *J. Am. Chem. Soc.,* 2019, **141**, 3833−3837.

[32] H. Y Sha, J. X. Xu, L. X. Huang, Z. Y. Xiong, Z. J. Wang, R. B. Su, C. He, X. M. Yang, X. F. Long, *Scr. Mater.,* 2022, **217**, 114764.

[33] T. H. Wu, X. X. Jiang, Y. R. Zhang, Z. J. Wang, H. Y. Sha, C. Wu, Z. S. Lin, Z. P. Huang, X. F. Long, M. G. Humphrey, C. Zhang, *Chem. Mater.,* 2021, **33**, 9317−9325.

[34] Y. L. Li, M. Y. Ji, C. L. Hu, J. Chen, B. X. Li, Y. Lin, J. G. Mao, *Chem.–Eur. J.,* 2022, **28**, e202200001.

[35] H. X. Tang, Y. X. Zhang, C. Zhuo, R. B. Fu, H. Lin, Z. J. Ma, X. T. Wu, *Angew. Chem. Int. Ed.,* 2019, **58**, 3824−3828.

[36] Q. Wei, C. He, K. Wang, X. F. Duan, X. T. An, J. H. Li, G. M. Wang, *Chem.–Eur. J.,* 2021, **27**, 5880−5884.

[37] X. H. Dong, L. Huang, H. M. Zeng, Z. E. Lin, K. M. Ok, G. H. Zou, *Angew. Chem. Int. Ed.,* 2022, **61**, e202116790.

[38] H. Li, H. T. Tian, C. S. Lin, X. Zhao, C. Wang, N. Ye, M. Luo, *Inorg. Chem.,* 2022, **61**, 19673−19677.

[39] Y. L. Han, X. Zhao, F. Xua, B. X. Li, N. Ye, M. Luo, *J. Alloys Compd.,* 2022, **902**, 163727.